Physical Controls on Phytoplankton Distribution in the Galápagos Archipelago

Megan Siwak, Temple University

Mentors: Giovanni Testa, Monique Messié

Summer 2026

Keywords: sea surface temperature, chlorophyll-a, phytoplankton, Galápagos Archipelago, island-driven upwelling, El Niño Southern Oscillation

ABSTRACT

The Galápagos Archipelago is a globally important hotspot of high productivity and biodiversity, primarily thanks to its location along the equator and its bathymetry contributing to strong island-driven upwelling. Despite this area undergoing long-term climatic changes, physical controls on phytoplankton distribution throughout the archipelago are poorly known on an interannual scale. Here, we investigate the impacts of island-driven upwelling and the El Niño Southern Oscillation (ENSO) on phytoplankton using satellite-based sea surface temperature and chlorophyll-a concentration products from September 1997 through December 2024. Our analysis uses sea surface temperature as a proxy for island-driven upwelling and for local ENSO impacts, and investigates the correlation between these physical factors and chlorophyll-a on both seasonal and interannual scales. Island-driven upwelling is associated with an increase in phytoplankton biomass. ENSO strength is associated with chlorophyll-a concentration, with El Niño events tending to demonstrate lower chlorophyll-a concentrations, and La Niña events showing higher concentrations. Advances in our understanding of the long-term impacts of physical controls on phytoplankton distributions are critical to predicting how life in coastal regions will respond to our changing climate.

INTRODUCTION

The equatorial Pacific Ocean is a hotspot of global ocean productivity, with the Galápagos archipelago being an especially productive region (Messié et al., 2022). The islands lie within the Galápagos Marine Reserve, where phytoplankton form the base of the ecosystem. Understanding phytoplankton conditions is therefore essential to understanding the reserve's changing ecological dynamics. Historically, studies on phytoplankton in this region focused on shorter term datasets and localized study regions. Recently, there have been an increase in efforts to study biophysics in the Galápagos archipelago regionally and over longer timescales (Forryan et al., 2021). With improving quantity and quality of satellite observations, studying the region interannually has been becoming easier.

Major physical phenomena controlling waters in this region include upwelling and El Niño Southern Oscillation events. Upwelling is defined as the movement of water from depths towards the surface. In the Galápagos archipelago, there are two types of upwelling, with both occurring via unique mechanisms. Equatorial upwelling occurs due to surface wind easterlies dragging water westwards, which is redirected away from the equator due to the Coriolis force. The resulting divergence draws deep waters, rich in nutrients and cold in temperature, up towards the surface. Island-driven upwelling occurs when waters moving toward a geologic platform hit the side and are forced upwards (De Falco et al., 2022). Here, the Equatorial Undercurrent moves eastwards from the central Pacific towards the archipelago. Island-driven upwelling is particularly strong off the west coast of Isabela and Fernandina, where the Equatorial Undercurrent hits the steep bathymetric slope of the islands and is forced upwards (Palacios, 2003). Both equatorial upwelling and island-driven upwelling play an important role in the region, but with different distributions. Equatorial upwelling is present at the equator, whereas island-driven upwelling is present off the western coast of Isabela and Fernandina. This feature is the primary driver behind the Island Mass Effect, which is the phenomenon of increased productivity in the area immediately surrounding an island (Gove et al., 2016).

El Niño Southern Oscillation (ENSO) is caused by a shift in a low pressure system typically residing over Indonesia. When this low pressure system shifts eastwards, a high pressure system typically over the eastern Pacific shifts westward, and conditions turn towards El Niño patterns. When El Niño conditions are present, the Galápagos tends to experience warming sea surface temperatures (McPhaden et al., 2006). As the climate system is tending towards

equilibrium, the low pressure system shifts westwards back towards its initial position; however, sometimes this location is overshot, and the low pressure system ends up being over the far western Pacific. This causes an eastward shift in the high pressure system toward the eastern Pacific, and in the Galápagos this leads to a cooling event (McPhaden et al., 2006). Sea surface temperature anomalies are a key indicator of ENSO phase and can also serve as a proxy for upwelling. Satellites have been continuously measuring sea surface temperature since 1980, providing a record that can be used to study historical upwelling and ENSO (Worsfold et al., 2024).

Physical oceanographic processes impact local nutrient conditions, which in turn impact phytoplankton biomass in a region. Chlorophyll-a is a green pigment found in all phytoplankton, and can thus be used as a proxy for phytoplankton biomass in marine environments. Satellites are able to detect chlorophyll-a due to their distinctive wavelength, and there has been a continuous record of global ocean chlorophyll-a mass concentration since 1997 (Garnesson et al., 2019). Here, sea surface temperature and chlorophyll-a data is analyzed in order to better understand physical controls on phytoplankton in the Galápagos.

METHODS

Datasets

Sea surface temperature (SST) data was from the Copernicus Marine Environmental Monitoring Service Global Ocean Operational SST and Sea Ice Analysis (OSTIA) SST and Sea Ice Reprocessed dataset. This is a L4 foundation sea surface temperature satellite product, taking in data from satellites operated by the European Space Agency Climate Change Initiative, Copernicus Climate Change Service, European Organization for the Exploitation of Meteorological Satellites, and Remote Sensing Systems, as well as in-situ input data from the Hadley Centre Integrated Ocean Database. At the time of access, this dataset was available from October 1, 1981 through December 18, 2025, with daily temporal and 0.05° spatial resolution.

Chlorophyll-a data was from the Copernicus Marine Environmental Monitoring Service Global Ocean Colour Bio-Geo-Chemical L4 from Satellite Observations product. This product takes in data from Sea-viewing Wide Field-of-view Sensor, Medium Resolution Imaging Spectrometer, Moderate Resolution Imaging Spectroradiometer on Aqua and Terra, Visible Infrared Imaging Radiometer Suite on Suomi NPP, JPSS-1/NOAA20, and JPSS-2/NOAA21, and

Ocean and Land Colour Instrument on S3A and S3B. At the time of access, this dataset was available from September 1997 through June 2026, with monthly temporal and 4 km spatial resolution.

The Niño Indices describe El Niño and La Niña in different regions of the equatorial Pacific (McPhaden et al., 2006). Niño 3.4, which uses variability from 5°N to 5°S and 170°W to 120°W, is often taken to represent the entire Pacific basin (McPhaden et al., 2006). Niño 3.4 SST Index from the NOAA ERSST V6 was downloaded from the NOAA Physical Sciences Laboratory website. The dataset based on ERSST V6 data was chosen as opposed to HadSST because ERSST V6 has a better representation of local dynamics varying on short timescales.

Focus Areas

Equatorial upwelling should have a consistent presence along the equator in areas west and east of the archipelago, while island-driven upwelling is present only west of the archipelago. The area spanning from -92.25 to -91.25°E, 0 to 1°S was chosen as the study region because its location as the first encounter between the Equatorial Undercurrent and the risen bathymetry of the islands makes it a hotspot for island-driven upwelling. The area spanning from -88 to -87°E, 0 to 1°S was chosen as the control region; because it shares the same latitude as the study area, the amount of equatorial upwelling should stay consistent. Additionally, because the Equatorial Undercurrent is not present here and there is no steep bathymetric gradient, there is no island-driven upwelling here.

Data Processing

To directly compare sea surface temperature and chlorophyll-a, the dataset resolutions had to be aligned. OSTIA was originally provided on a daily scale, so monthly averages were taken from September 1997 through December 2024, in accordance with Copernicus GlobColour. Additionally, the spatial resolutions differed across datasets. Because Copernicus GlobColour uses a finer resolution than OSTIA in this region, a conservative regridding function was applied to Copernicus GlobColour output in order to match the 0.05 degree resolution of OSTIA.

Ocean color products have known patterns of interference with the seafloor in shallow coastal regions. To avoid this phenomenon influencing the results, a mask was applied to the Copernicus GlobColour product such that any pixels containing a bathymetry of 30 m or less were excluded. This metric was applied following Messié et al. (2022) and using the GEBCO

(General Bathymetric Chart of the Oceans) database. For continuity, the same mask was applied to OSTIA.

RESULTS

The linear regression between satellite-estimated sea surface temperature and chlorophyll-a is shown in Figure 1. Mean conditions (Figure 2), seasonal cycles (Figure 3), and interannual trends (Figures 4 and 5) are also presented. The regression between chlorophyll-a and the Niño 3.4 index is shown in Figure 6, while the time series of the coherence between the two datasets is presented in Figure 7. The results of the empirical orthogonal function analysis are shown in Figures 8–10.

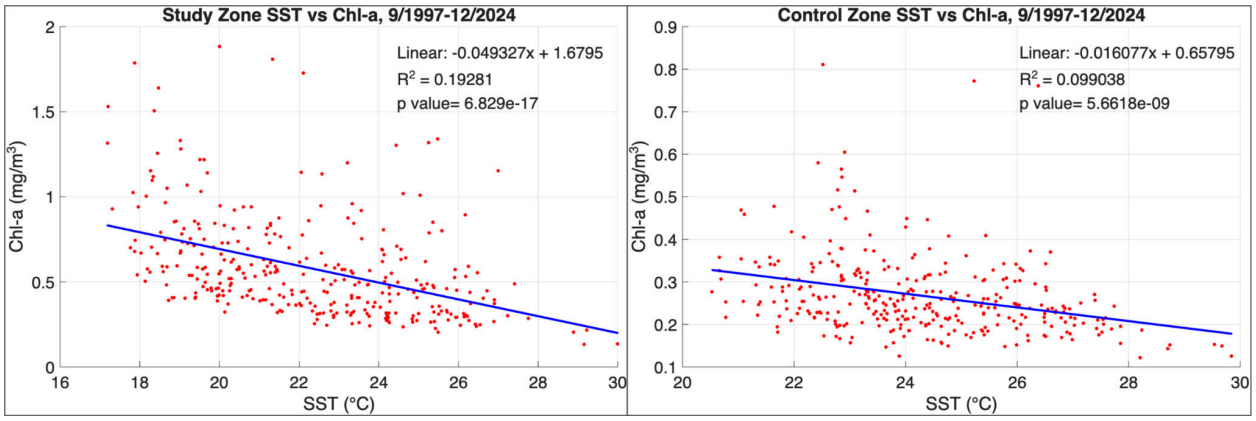


Figure 1. Linear regression between monthly sea surface temperature and chlorophyll-a mass concentration for the study (left) and control (right) regions. For both regions, there is a statistically significant, low precision, negative relationship between sea surface temperature and chlorophyll-a. This relationship is stronger in the study zone than in the control zone.

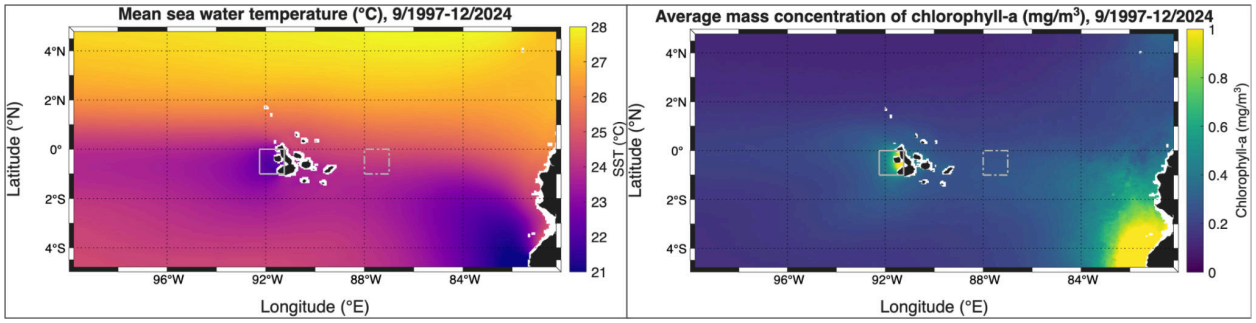


Figure 2. Average sea surface temperature (left) and chlorophyll-a mass concentration (right). The study area is bounded by the solid gray box, and the control area is bounded by the dot-dash gray box.

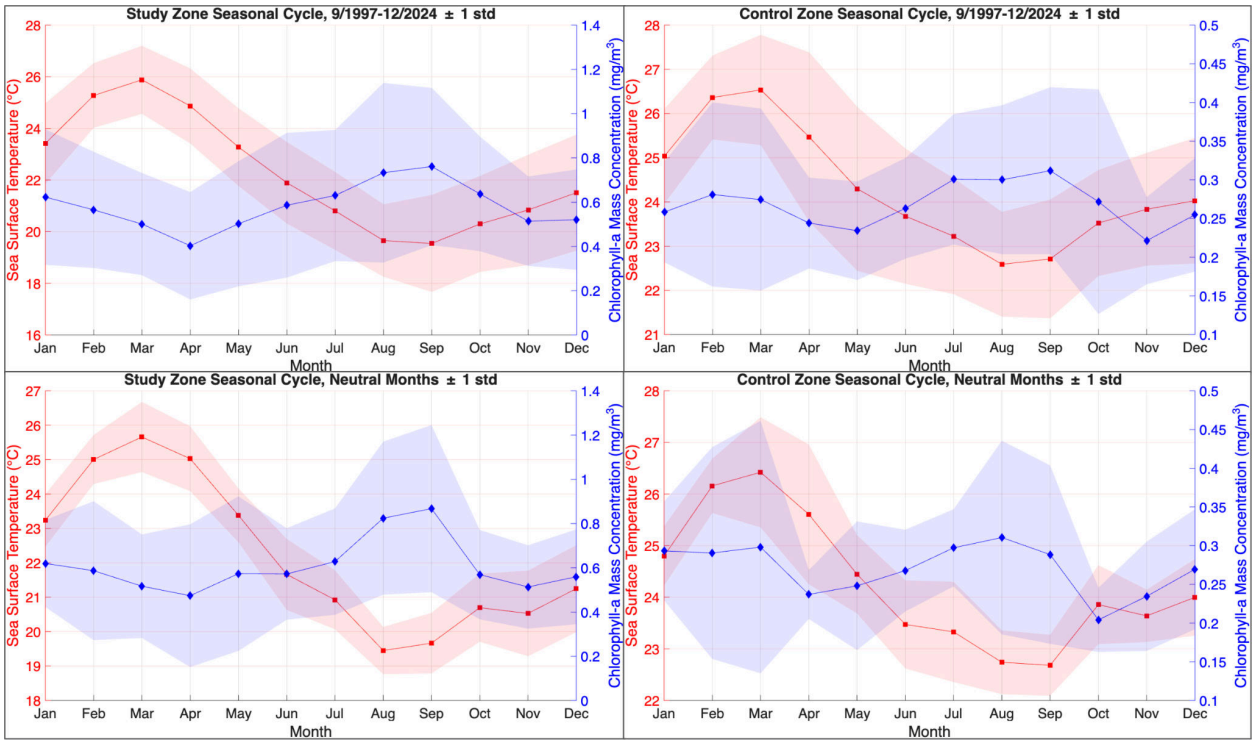


Figure 3. Seasonal cycle of sea surface temperature and chlorophyll-a mass concentration for the full timeseries (top) and neutral months (bottom, defined as having a Nino 3.4 index of between -0.5 and 0.5°C) for the study (left) and control (right) regions. Sea surface temperature reaches a maximum in March and minimum in August or September. Chlorophyll-a reaches a maximum in August or September, but the month of minimum concentration differs greatly across all four focuses.

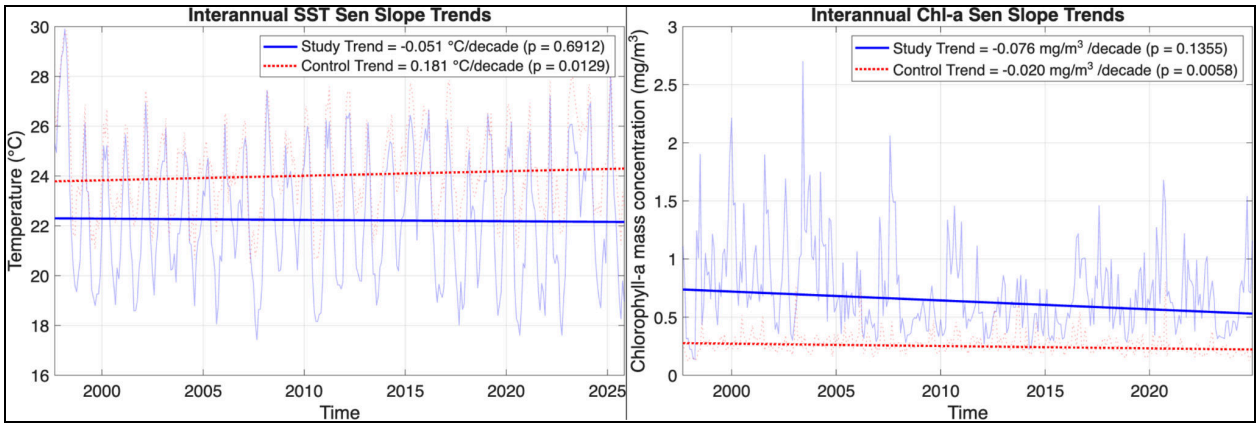


Figure 4. Interannual trends for sea surface temperature (left) and chlorophyll-a (right) as determined by a Sen slope and Mann-Kendall test, for the study and control regions.

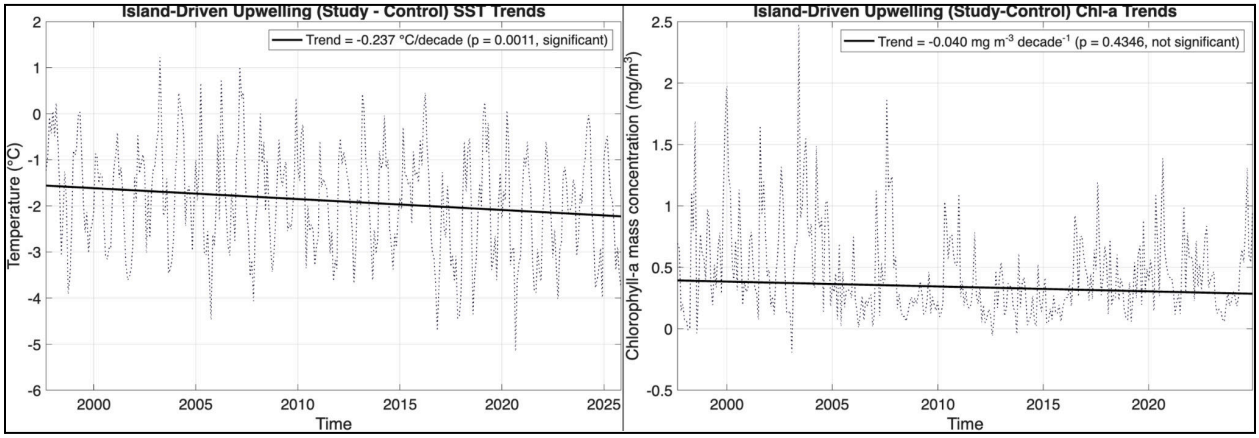


Figure 5. Island-driven upwelling, calculated as Sen slope and Mann-Kendall test of the study minus the control, as seen with sea surface temperature (left) and chlorophyll-a (right).

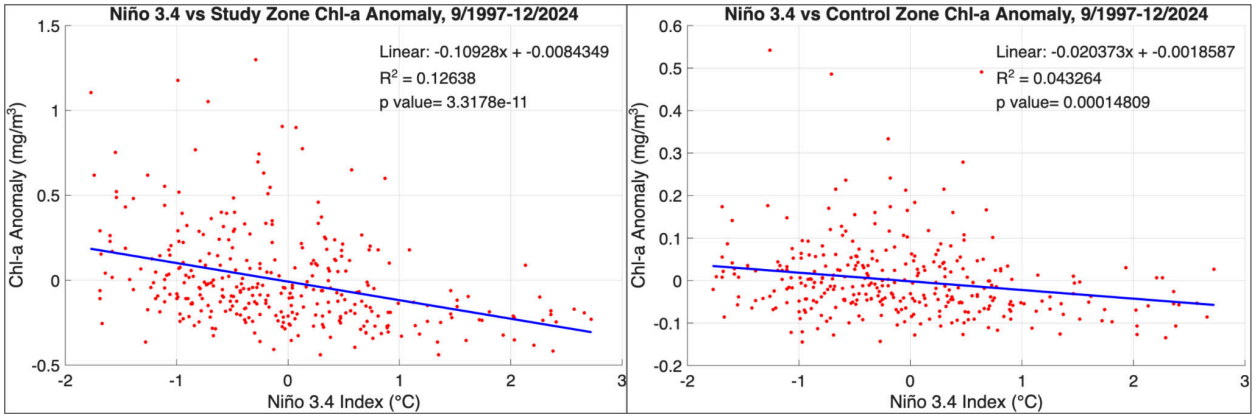


Figure 6. Linear regression between Nino 3.4 index and chlorophyll-a anomaly for the study (left) and control (right) regions. For both regions, there is a statistically significant, low precision, negative relationship between the Nino 3.4 index and chlorophyll-a. This relationship is stronger in the study zone than in the control zone.

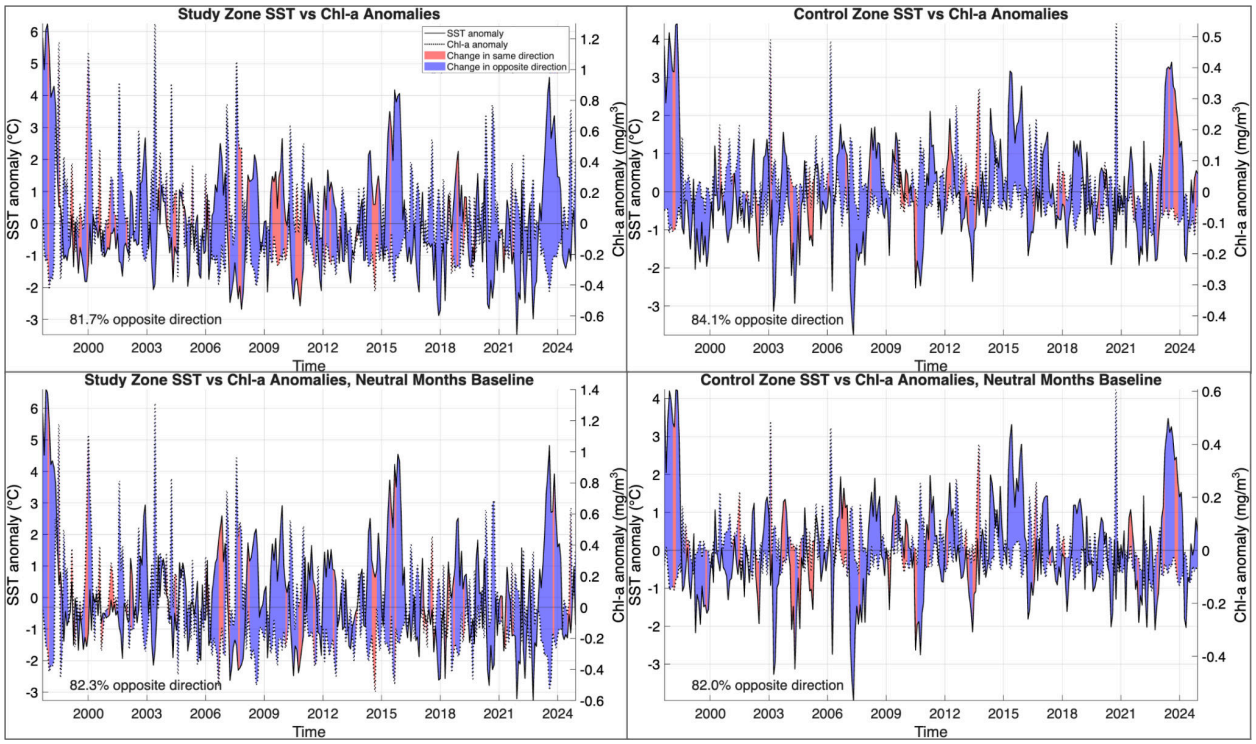


Figure 7. Monthly sea surface temperature and chlorophyll-a concentration anomalies using the full timeseries seasonal cycle (top) and neutral month seasonal cycle (bottom, defined as having a Nino 3.4 index of between -0.5 and 0.5°C) for the study (left) and control (right) regions.

Similar directions of anomalies were shaded in red, while dissimilar directions were shaded in blue.

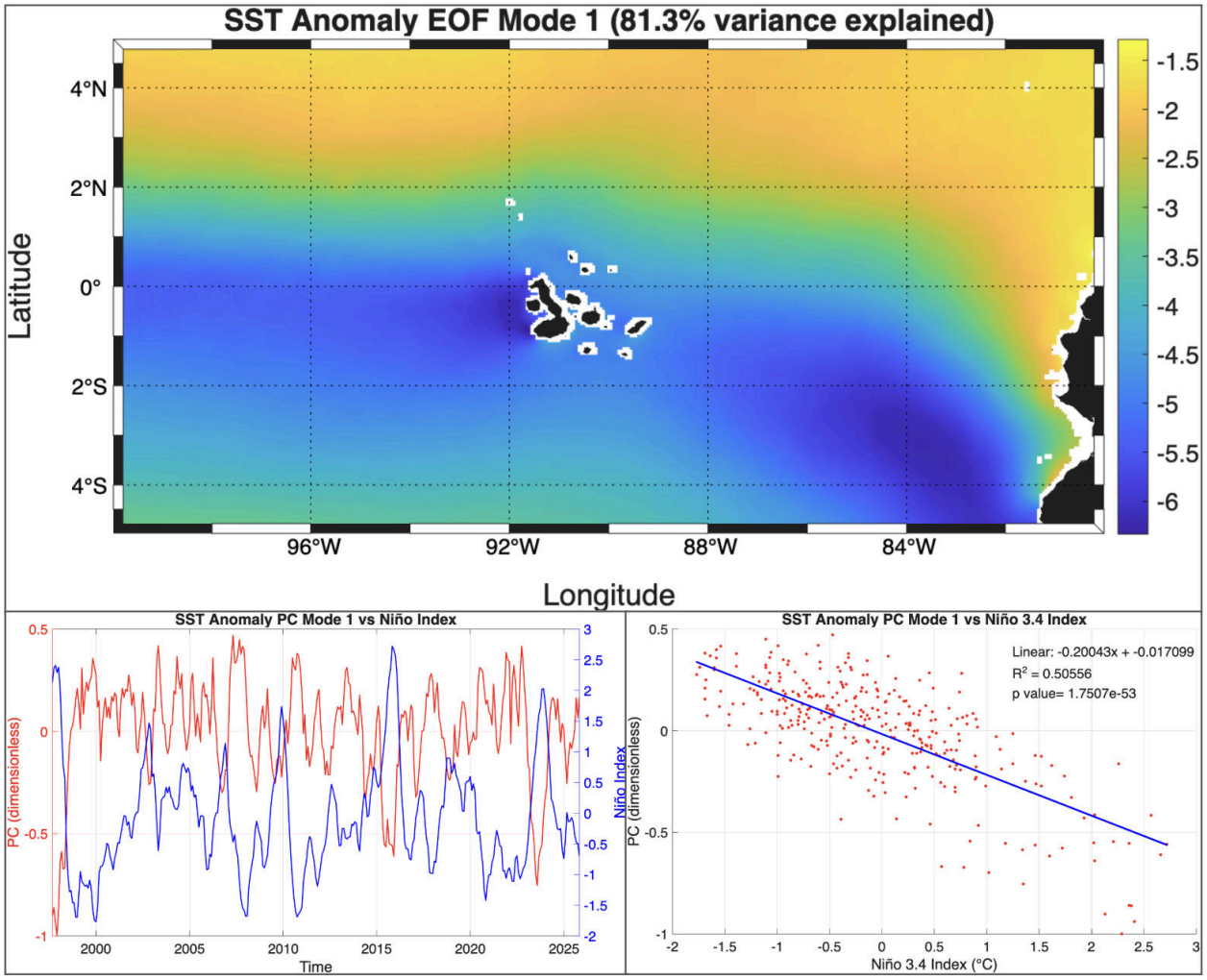


Figure 8. Empirical orthogonal function of sea surface temperature anomaly (top), and principal component vs Nino Index direct comparisons (bottom left) and linear regression (bottom right). The high p-value and moderate correlation suggests that the first mode of sea surface temperature variability is due to ENSO.

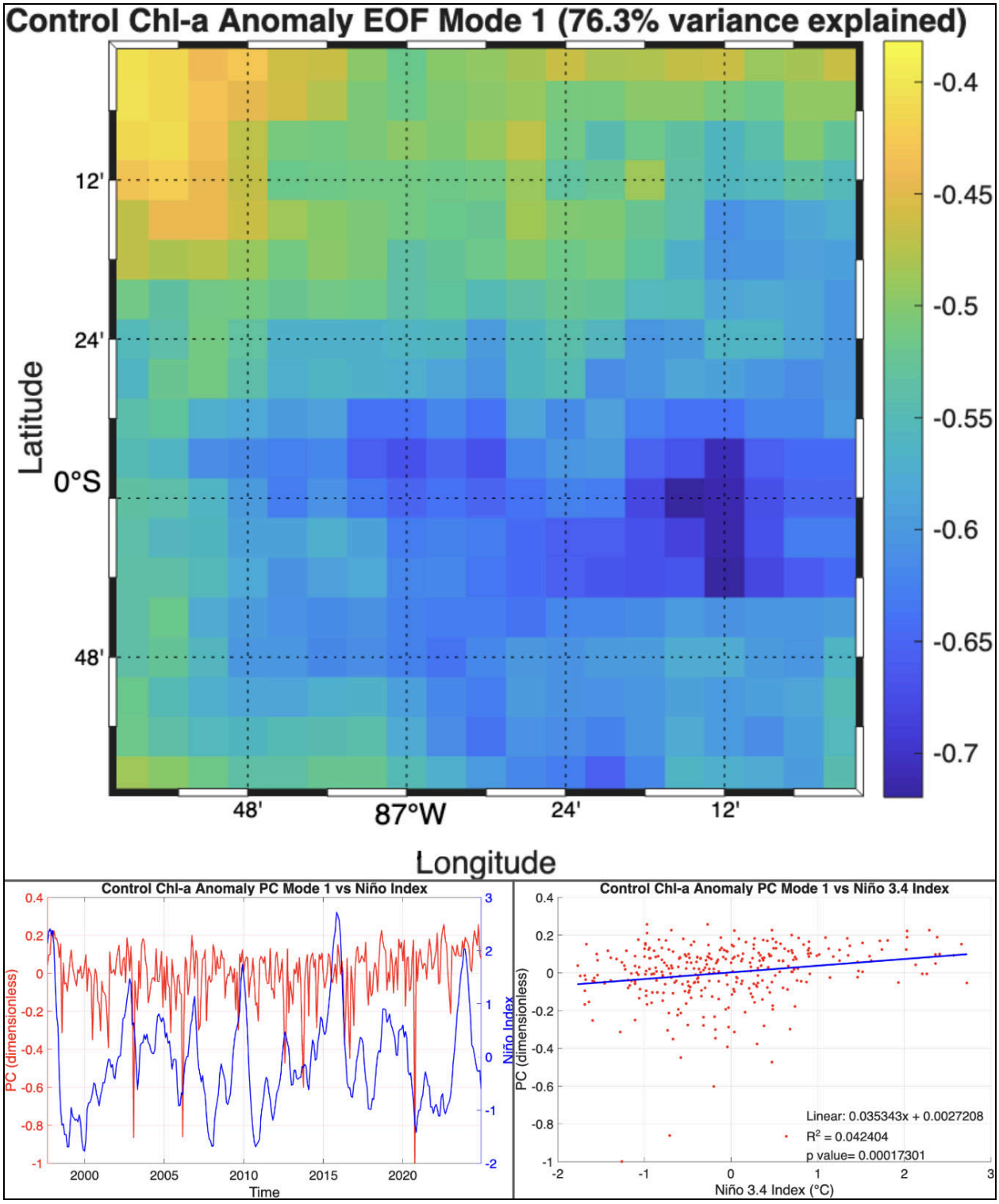


Figure 9. Empirical orthogonal function of chlorophyll-a mass concentration anomaly (top), and principal component vs Nino Index direct comparisons (bottom left) and linear regression (bottom right) for the control region.

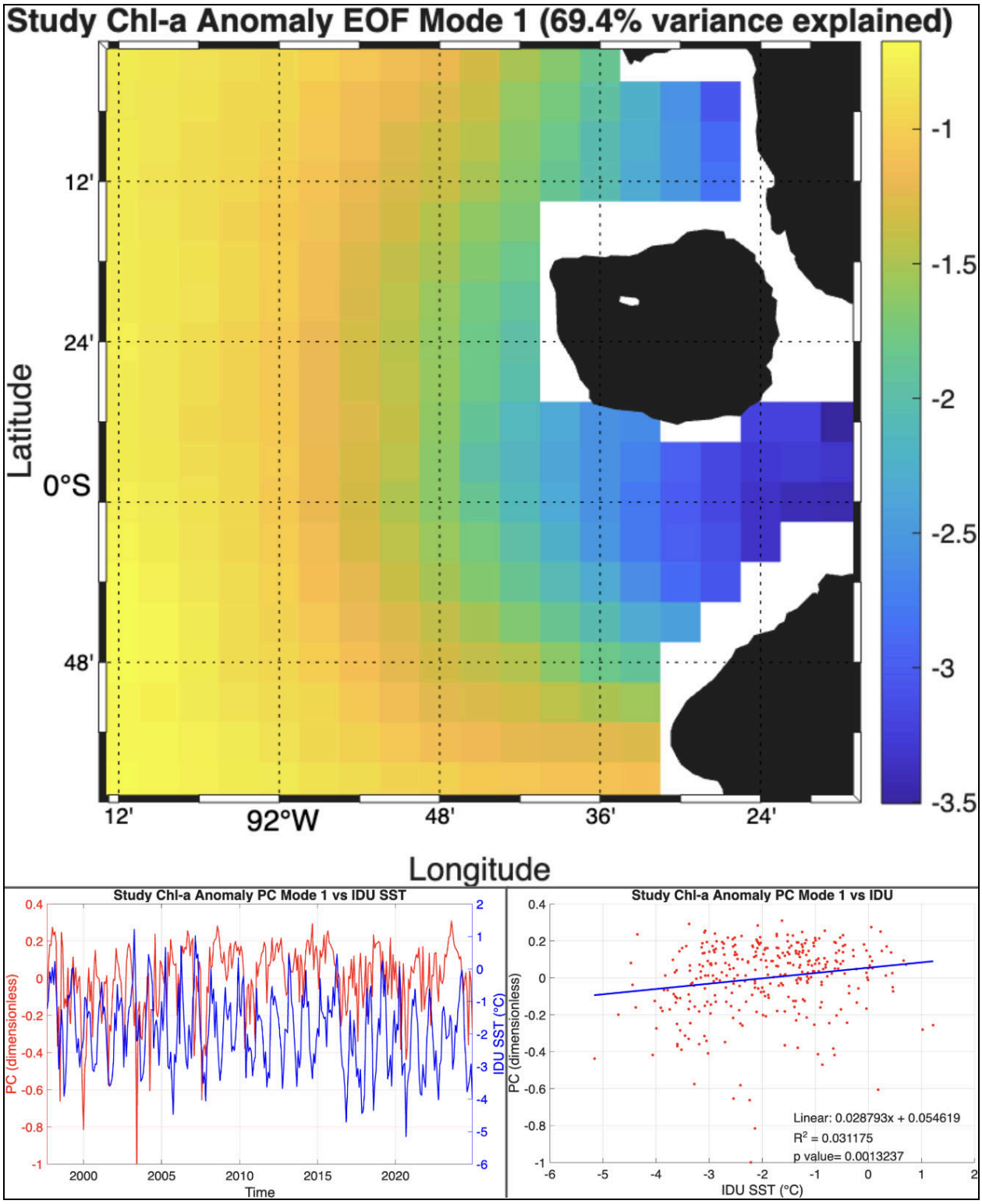


Figure 10. Empirical orthogonal function of chlorophyll-a mass concentration anomaly (top), and principal component vs island-driven upwelling sea surface temperature direct comparisons (bottom left) and linear regression (bottom right) for the study region.

DISCUSSION

In this region, low sea surface temperatures can be expected to correlate with nutrient-rich, and thus chlorophyll-a-rich and phytoplankton-rich, waters. A linear regression comparing sea surface temperature and chlorophyll-a measurements for both study and control regions shows a statistically significant but weak negative relationship between the two variables (Figure 1). While the relationship is significant, its weakness suggests that the link between temperature and phytoplankton is more complex than a simple linear relationship captures. This foundational relationship is apparent when looking at spatial and temporal patterns of sea surface temperature and chlorophyll-a, as seen in Figures 2 and 3. In the region, temperature is highest in a band north of the equator, aligned with the northern boundary of the Equatorial Front. While the region south of the equator is generally cooler, there are regions of extremely cold water off the coast of Ecuador, and west of Fernandina and Isabela. Cooling off the coast of Ecuador is associated with the Humboldt Current. The study region, known to be conducive to island-driven upwelling, lies within a cool tongue extending westwards of the archipelago. The control region lies along the boundary of the Equatorial Front, north of the primary Humboldt cooling. In contrast to the sea surface temperature, chlorophyll-a shows a similar distribution of extreme values. The Equatorial Front is not visible in the chlorophyll-a plot. High concentrations appear in the same locations of extremely cold waters: off the coast of Ecuador, and west of Fernandina and Isabela. The seasonal cycle distribution complicates the picture further. For both zones, and for both the full timeseries and only the neutral months (excluding El Niño and La Niña events), sea surface temperature shows a maximum in March and a minimum in August or September. Chlorophyll-a, though far more variable, shows a maximum in August or September, and a minimum usually between March and April: opposite of sea surface temperature. Neutral seasonal cycles tend to show more variability in the magnitude of standard deviation per month, which may be due to the amount of neutral instances differing per month.

El Niño and La Niña events have different effects on chlorophyll-a mass concentrations, as seen in Figure 6. Despite a weak correlation, there is a statistically significant negative relationship between the Niño 3.4 Index and chlorophyll-a anomaly calculated from the full timeseries: in El Niño years there tends to be a negative chlorophyll-a anomaly, whereas in La Niña years there tends to be a positive anomaly. This relationship is much stronger in the study

zone than in the control zone, and shows a higher spread in La Niña months than in El Niño months.

When looking at the full timeseries, the interannual trends for sea surface temperature don't fully align with those of chlorophyll-a, seen in Figure 5. For sea surface temperature, the study area experiences an insignificant decrease in temperature, while the control area experiences a significant, strong increase. The more central control region has been warming since 1997. Given the inverse relationship between sea surface temperature and chlorophyll-a, it is expected that chlorophyll-a concentrations will experience an insignificant increase in the study area and a significant decrease in the control area. The expected pattern is present with the control region, though the decrease is very small. In the study zone, however, there is a statistically insignificant, strong decrease in chlorophyll-a. To evaluate the effect of island-driven upwelling on this relationship, island-driven upwelling was calculated as the study variable minus the control variable (Figure 5). Any difference between the two should be the result of island-driven upwelling because that is the major oceanographic difference between the two areas. For sea surface temperature, there is a significant, strong increase in island-driven upwelling. When the same calculation was applied to chlorophyll-a, there is a statistically insignificant, slight decrease in chlorophyll-a concentrations. While the major physical difference in water movement between the two regions is the presence of island-driven upwelling, the disconnect between sea surface temperature and chlorophyll-a suggests that island-driven upwelling is not the only driver of chlorophyll-a distributions in the study area.

A direct comparison of the Niño 3.4 Index and chlorophyll-a anomaly for both the study and control zones is displayed in Figure 6, showing a statistically significant but weak negative relationship. The study zone shows a stronger correlation than the control zone. Because both the study and control zones lie outside of the Niño 3.4 region, the correlation might be improved by choosing a mix of Niño 1+2 and Niño 3 indices. Regardless, chlorophyll-a tends to be lower in months that are characterized as El Niño, and higher in months that are characterized as La Niña.

Since ENSO is typically quantified on the basis of sea surface temperature anomalies, a more direct comparison for each region would be to compare sea surface temperature anomalies and chlorophyll-a anomalies. Figure 7 shows this direct comparison for both anomalies calculated using the full timeseries, and anomalies calculated using only months with a Niño 3.4 Index between -0.5° and 0.5°C. Given the relationship established from Figure 1, it is expected

that as sea surface temperature anomaly increases, chlorophyll-a mass concentration anomaly decreases, and vice versa. This expected pattern occurs between 81.7%-84.1% of the time. The neutral month baseline shows a much closer pattern across zones, ranging from 82.0% to 82.3%, suggesting that ENSO is responsible for the difference across zones. ENSO does not explain the unexpected pattern of sea surface temperature anomalies and chlorophyll-a mass concentration anomalies moving in the same direction, though.

To better dissect the causes of variability on spatial and temporal scales, an empirical orthogonal function analysis was performed. Sea surface temperature anomalies showed one dominant mode across the entire region, explaining 81.3% of the variability. A comparison between the principal component of mode 1 and the Niño 3.4 Index in Figure 8 shows a significant negative relationship, with a higher correlation than any regression seen previously, suggesting that ENSO is responsible for most sea surface temperature variability. Chlorophyll-a is messier to disentangle. The two regions were analyzed independently. The control zone experiences a greater magnitude of change in the southeast quadrant of Figure 9 (top image). The spatial distribution suggests that the primary driver for this mode could be a current or front. An analysis of the control zone chlorophyll-a anomaly principal component of mode 1 versus the Niño Index shows a statistically significant but weak positive relationship. This weak-but-significant relationship suggests that ENSO likely contributes to this feature but is not its sole cause. An identical analysis was conducted for the study zone chlorophyll-a anomalies against island-driven upwelling sea surface temperature differences. The spatial distribution seen in the top of Figure 10 shows that this phenomenon is strongest closest to the coast. Strangely, a linear regression between the two also shows a statistically significant but weak positive relationship, suggesting that island-driven upwelling contributes to, but is not the sole driver of, this phenomenon.

CONCLUSIONS

Sea surface temperature was used as a proxy for ENSO and upwelling, and chlorophyll-a mass concentration as a proxy for phytoplankton biomass, in a comparison between an island-driven upwelling region of the Galápagos and a comparable region without island-driven upwelling. While a significant negative relationship exists between sea surface temperature and

chlorophyll-a, neither ENSO, as defined by the Niño 3.4 Index, nor island-driven upwelling fully accounts for the chlorophyll-a trends observed.

Many questions remain about the biophysics of this region. Unexpected chlorophyll-a trends may stem from technical issues, such as satellite data processing and calculation methods, or from physical dynamics not examined in this analysis, such as the position of the Equatorial Front. The most pertinent next step is to repeat this analysis using the Niño 1+2 and Niño 3 Indices, as localized ENSO events are likely more relevant to localized chlorophyll-a concentrations than broader basin-wide indices.

ACKNOWLEDGEMENTS

Thank you to Giovanni Testa and Monique Messié for their mentorship and guidance throughout this project. This was all made possible by the MBARI Summer Internship Program, and I'd like to thank George Matsumoto, Megan Bassett, and Jessica Chapman for their time and efforts in organizing this program, and to the MBARI staff for creating such a welcoming environment. The MBARI Summer Internship Program is generously supported through a gift from the Dean and Helen Witter Family Fund and the Rentschler Family Fund in memory of former MBARI board member Frank Roberts (1920-2019) and by the David and Lucile Packard Foundation. Additional funding is provided by Dalio Philanthropies and the Maxwell/Hanrahan Foundation.

REFERENCES

Behrenfeld, M.J., R.T. O'Malley, D.A. Siegel, C.R. McClain, J.L. Sarmiento, G.C. Feldman, A.J. Milligan, P.G. Falkowski, R.M. Letelier, and E.S. Boss. 2006. Climate-driven trends in contemporary ocean productivity. *Nature,* 444:752-755. https://doi.org/10.1038/nature05317

Browning, T.J. and C.M. Moore. 2023. Global analysis of ocean phytoplankton nutrient limitation reveals high prevalence of co-limitation. *Nature Communications,* 14:5014. https://doi.org/10.1038/s41467-023-40774-0

Chavez, F., and R.C. Brusca. 1991. The Galápagos Islands and their relation to oceanographic processes in the tropical Pacific. Pp. 9-33 in *Galápagos Marine Invertebrates*. M. J. James, ed. Springer, New York, NY.

De Falco, C., F. Desbiolles, A. Bracco, and C. Pasquero. 2022. Island mass effect: a review of oceanic physical processes. *Frontiers in Marine Science,* 9:894860. https://doi.org/10.3389/fmars.2022.894860

E.U. Copernicus Marine Service Information (CMEMS). 2022. *Product User Manual for the Global Ocean OSTIA Sea Surface Temperature Reprocessing product*, SST-GLO-SST-L4-REP-OBSERVATIONS-010-011. Ref: SST-PUM-010-002-011, Issue 1.4. Mercator Ocean International, Toulouse, France. https://documentation.marine.copernicus.eu/PUM/CMEMS-SST-PUM-010-011.pdf

E.U. Copernicus Marine Service Information (CMEMS). 2026. *Quality Information Document for the Global Ocean OSTIA Sea Surface Temperature Reprocessing Product*, SST-GLO-SST-L4-REP-OBSERVATIONS-010-011. Ref: CMEMS-SST-QUID-010-011, Issue 4.0. Mercator Ocean International, Toulouse, France. https://documentation.marine.copernicus.eu/QUID/CMEMS-SST-QUID-010-011.pdf

E.U. Copernicus Marine Service Information (CMEMS). 2026. *Product User Manual for Ocean Colour Products*, OCEANCOLOUR_GLO_BGC_L4_MY_009_104. Ref: CMEMS-OC-PUM-7.0, Issue 7.0. Mercator Ocean International, Toulouse, France. https://documentation.marine.copernicus.eu/PUM/CMEMS-OC-PUM.pdf

Forryan, A., A.C. Naveira Garabato, C. Vic, A.J.G. Nurser, and A.R. Hearn. 2021. Galápagos upwelling driven by localized wind-front interactions. *Scientific Reports,* 11:1277. https://doi.org/10.1038/s41598-020-80609-2

Garnesson, P., A. Mangin, O. Fanton d'Andon, J. Demaria, and M. Bretagnon. 2019. The CMEMS GlobColour chlorophyll a product based on satellite observation: Multi-sensor merging and flagging strategies. *Ocean Science,* 15(3):819–830. https://doi.org/10.5194/os-15-819-2019

Gove, J.M., M.A. McManus, A.B. Neuheimer, J.J. Polovina, J.C. Drazen, C.R. Smith, M.A. Merrifield, A.M. Friedlander, J.S. Ehses, C.W. Young, A.K. Dillon, G.J. Williams. 2016. Near-island biological hotspots in barren ocean basins. *Nature Communications,* 7:10581. https://doi.org/10.1038/ncomms10581

McPhaden, M.J., S.E. Zebiak, and M.H. Glantz. 2006. ENSO as an integrating concept in earth science. *Science,* 314:1740-1745. https://doi.org/10.1126/science.1132588

Messié, M., A. Petrenko, A.M. Doglioli, E. Martinez, and S. Alvain. 2022. Basin-scale biogeochemical and ecological impacts of islands in the tropical Pacific Ocean. *Nature Geoscience,* 15:469-474. https://doi.org/10.1038/s41561-022-00957-8

Moore, C.M., M.M. Mills, K.R. Arrigo, I. Berman-Frank, L. Bopp, P.W. Boyd, E.D. Galbraith, R.J. Geider, C. Guieu, S.L. Jaccard, T.D. Jickells, J. La Roche, T.M. Lenton, N.M. Mahowald, E. Marañón, I. Marinov, J.K. Moore, T. Nakatsuka, A. Oschlies, M.A. Saito, T.F. Thingstad, A. Tsuda and O. Ulloa. 2013. Processes and patterns of oceanic nutrient limitation. *Nature Geoscience,* 6:701-710. https://doi.org/10.1038/NGEO1765

Palacios, D. 2002. Factors influencing the island-mass effect of the Galápagos Archipelago. *Geophysical Research Letters,* 29(23):2134. https://doi.org/10.1029/2002GL016232

Palacios, D. 2003. Seasonal patterns of sea-surface temperature and ocean color around the Galápagos: regional and local influences. *Deep-Sea Research II,* 51:43-57. https://doi.org/10.1016/j.dsr2.2003.08.001

Worsfold, M., S. Good, C. Atkinson, and O. Embury. 2024. Presenting a long-term, reprocessed dataset of global sea surface temperature produced using the OSTIA system. *Remote Sensing,* 16:3358. https://doi.org/10.3390/rs16183358